Article

Low-Carbon Truck-Multi-Drone Collaborative Routing for Urban Cold-Chain Distribution with Perishability and Time-Varying Payloads

Fangyan Ma[1,*] and Longcan Wang[1]

[1] Hainan Vocational University of Science and Technology, Haikou, China
* Correspondence: Fangyan Ma, Hainan Vocational University of Science and Technology, Haikou, China

Abstract: Rapid grocery and fresh-food fulfilment requires delivery systems that reconcile operating cost, product freshness, service reliability, and environmental performance. Conventional truck-only routing is vulnerable to congestion and road closures, whereas stand-alone drones remain constrained by payload, endurance, launch and recovery requirements, and regulated airspace. This study formulates a multi-objective truck-multi-drone routing problem for urban cold-chain distribution incorporating simultaneous delivery and pickup, split service, soft time windows, ground blockages, no-fly arcs, truck-drone synchronization, exponential quality decay, and payload-dependent operational emissions. The three objectives minimize economic fulfilment cost, monetized freshness loss, and operational carbon dioxide equivalent emissions. A multi-objective adaptive large-neighborhood search (MO-ALNS) is developed around a bounded nondominated archive, crowding-based diversity control, adaptive operator selection, and problem-specific destroy and repair operators addressing high-loss customers, restriction boundaries, split-demand structures, safe air insertion, and launch-rendezvous synchronization. A Manhattan-calibrated scenario is used to evaluate the formulation. Relative to truck-only delivery, the collaborative configuration reduces total fulfilment cost by 18.70%, freshness-loss cost by 42.30%, operational emissions by 17.51%, and the time-window violation rate by 26.3 percentage points. Representative Pareto solutions expose a clear cost-freshness-carbon trade-off, while carbon-price scenarios indicate a shift toward higher drone participation and earlier unloading of high-demand customers. Against NSGA-II, MO-ALNS produces a 14.2% higher hypervolume and a 24.4% lower generational distance. Stress tests further demonstrate that the collaborative network contains severe congestion more effectively than truck-only routing, supporting payload-aware, restriction-aware routing as a practical basis for resilient low-carbon cold-chain planning.

Keywords: cold-chain logistics; vehicle routing; truck-drone collaboration; multi-objective optimization; carbon emissions; perishability

Received: 23 June 2026
Revised: 30 July 2026
Accepted: 14 August 2026
Published: 19 August 2026

1. Introduction

The last mile of urban cold-chain distribution is unusually demanding because time, temperature, and movement are tightly coupled [1]. A late delivery is not merely a service failure: it can accelerate product deterioration, reduce saleable shelf life, and increase the likelihood of disposal. At the same time, dense urban environments expose refrigerated vehicles to recurrent congestion, limited curb access, temporary road restrictions, and highly fragmented order patterns. The planner must therefore coordinate routing, timing, capacity, and product condition rather than minimize distance alone. These pressures are especially pronounced in rapid grocery and fresh-food fulfilment, where customers expect narrow delivery windows and retailers must protect both operational margin and product freshness.

Truck-drone collaboration offers a potential response. A truck supplies range, payload capacity, refrigeration, and a mobile launch platform, while drones can bypass congested streets and serve light, time-sensitive orders directly [2]. Foundational studies on flying-sidekick and traveling-salesman-with-drone frameworks demonstrate how launch, service, and rendezvous decisions can be integrated with a ground route. Later exact and heuristic methods indicate that synchronization is the defining challenge of this problem class. Drone routing research also shows that endurance is not a fixed geometric radius: energy use depends on payload, speed, airframe design, and mission phase. Consequently, an operationally credible cold-chain model must coordinate two networks and two energy systems rather than treat a drone as a cost-free shortcut.

Environmental assessments require similar rigor. Small drones may reduce energy use for light parcels in appropriate settings, but their advantage depends on electricity carbon intensity, package mass, flight distance, and supporting infrastructure. For trucks, fuel consumption depends not only on distance but also on speed, acceleration, road conditions, and payload. This matters in simultaneous delivery and pickup operations because truck load changes after every service. A distance-only emission coefficient assigns the same footprint to an empty return arc and a heavily loaded outbound arc, obscuring the operational effect of service sequence [2]. Such an approximation can also obscure a useful routing mechanism: serving a large delivery early may be environmentally beneficial even when it marginally increases distance, because the truck travels subsequent arcs at a lower mass.

Freshness introduces a third criterion requiring careful integration. Perishable-food routing studies have incorporated time-dependent travel, soft or hard time windows, temperature-dependent deterioration, and freshness-related cost. Their results consistently show that a route with the lowest transport cost need not deliver the freshest product [3]. This integration becomes more complex when drones are added. More drone sorties can shorten customer response times, yet they add launch, recovery, electricity, and synchronization costs. Likewise, a carbon-oriented sequence may favor early unloading of large orders, whereas a freshness-oriented sequence may prioritize products with high decay rates or customers with tight windows. Reducing the three criteria to a single weighted sum before optimization can obscure non-convex regions of the decision space and makes the selected solution sensitive to arbitrary weight assignments.

This paper addresses these interactions through a tri-objective formulation and a tailored solution procedure. The problem includes a depot, refrigerated trucks, multiple truck-carried drones, customer-level delivery and pickup quantities, divisible demand, soft time windows, time-dependent ground travel, restricted ground and air arcs, drone endurance, and truck-drone launch and recovery synchronization. Product value declines according to a first-order exponential function. Operational emissions include payload-dependent truck fuel use and electricity-related drone emissions, with an explicit accounting boundary. The model is solved using a multi-objective adaptive large-neighborhood search (MO-ALNS) that maintains a nondominated archive instead of collapsing all criteria into a predetermined scalar score [4].

The contribution is fourfold. First, the model unifies ground access limitations and airspace restrictions in a single multimodal feasibility structure, enabling the two modes to compensate for different spatial limitations. Second, it propagates truck payload after each simultaneous delivery-and-pickup event and links that state to arc-level fuel use and emissions. Third, it separates economic cost, freshness loss, and carbon emissions while using a posteriori Pareto analysis to support decision making. Fourth, it develops restriction-aware and split-service-aware ALNS operators that repair the structural causes of infeasibility rather than relying exclusively on generic mutation [5].

The numerical evidence is a calibrated scenario analysis, not a field trial. The source manuscript provides aggregate performance tables, model outputs, and source categories, but it does not include customer-level commercial orders, complete road matrices, executable code, hardware specifications, or run-level observations. Accordingly, the reported values are preserved and analyzed as author-supplied scenario outputs [6]. Statements of statistical significance, universal superiority, and direct operational readiness are avoided. This distinction strengthens the evidentiary boundary of the study and identifies the artifacts required for reproducibility.

2. Related Literature and Research Gap

2.1. Truck-Drone Collaborative Routing

Early formulations introduced delivery-by-drone configurations where a drone is launched from and recovered by a delivery truck. Subsequent work developed traveling salesman problem variants incorporating drones, along with route-first, cluster-second solution approaches. These studies established core decision elements: customer assignment across transport modes, drone launch and recovery locations, and coordination of waiting times between truck and drone operations. Later advances demonstrated that exact methods can address larger problem instances through dynamic programming and branch-and-price techniques [7]. A shift in objective function occurred toward minimizing operating cost, with explicit modeling of waiting costs within a minimum-cost traveling salesman problem framework involving drones.

The body of work has since extended to settings involving multiple trucks and multiple drones, time windows, pickup-and-delivery requirements, payload-dependent energy consumption, and airspace constraints. Empirical analysis confirmed that drone battery capacity and payload must be jointly considered to ensure route feasibility. Multi-drone configurations enhance operational parallelism but introduce coordination requirements at shared launch and recovery points; recent exact methods confirm that these variants remain computationally challenging even without incorporating perishability or ground traffic congestion. Survey analyses indicate that much of the existing literature still relies on simplified assumptions—such as single-truck/single-drone configurations, fixed Euclidean distances, unrestricted airspace, or basic customer assignment rules [8].

For urban deployment, prohibited ground and air movements must be excluded from the feasible graph rather than penalized generically. Regulatory distinctions exist between airspace restrictions and localized take-off and landing limitations; thus, an optimized route serves only as a planning candidate and does not constitute operational authorization [9].

2.2. Perishable-Food Routing and Simultaneous Pickup and Delivery

Classical vehicle routing with time windows follows the benchmark structure established in foundational work on the topic. Simultaneous pickup and delivery extends the state space because vehicle load may decrease after delivery and increase again after pickup. Specialized route evaluation and neighborhood search are required for such flows; feasibility cannot be inferred from total route demand alone, as the maximum payload may occur at an intermediate customer [10].

Cold-chain routing introduces quality dynamics. Time-dependent travel and product deterioration have been incorporated into perishable-food distribution models. Perishability has also been explicitly treated as a distribution cost in applications involving fresh vegetables, with time-dependent routing applied accordingly. The cost-freshness relationship has been formulated as a multi-objective problem, demonstrating that freshness is not adequately captured by distance or lateness alone [3]. These considerations motivate a separate freshness objective and a nonlinear decay function.

Nevertheless, freshness models and truck-drone models are often developed independently. A drone may reduce elapsed time for a small delivery, but the truck may need to wait at the rendezvous point, thereby delaying service to other customers. A split order further complicates quality calculation, as truck-carried and drone-carried portions may arrive at different times [11]. A rigorous formulation therefore associates deterioration with the service time of each delivered portion rather than with a single route-level completion time. This paper adopts that portion-specific interpretation and treats pickup quantities as capacity flows rather than as fresh product delivered to the customer.

2.3. Payload-Dependent Carbon and Drone Energy

The pollution-routing problem formalizes the joint influence of routing, speed, payload, and time on freight emissions [12]. Subsequent adaptive large neighborhood search approaches demonstrated that emissions-aware route and speed decisions can be solved effectively for practical instances, while broader reviews emphasize that emission estimates depend critically on the selected physical or empirical model. A common reduced-form model interpolates between an empty-vehicle consumption rate and a full-load rate. Although this approximation does not capture transient acceleration effects or refrigeration-unit energy demand, it preserves an important operational relationship: fuel consumption on a given arc increases with payload.

Drone emissions are indirect under battery-electric operation and depend on total energy consumed and the carbon intensity of the electricity grid. Life-cycle analyses indicate that small drones may outperform trucks for light-package delivery in appropriately designed systems; however, additional warehousing requirements or deployment of larger aircraft can reverse this advantage. Empirical flight studies confirm the sensitivity of drone energy consumption to both payload and speed. Integrated modeling has linked drone routing decisions to operational cost and carbon performance, while truck-based comparisons show that environmental outcomes hinge on the choice of ground-transport benchmark and the defined system boundary. Consequently, it is not valid to assume uniform environmental superiority of drone kilometers over truck kilometers.

The present model reports operational CO_2-equivalent emissions: direct fuel-related emissions from trucks plus electricity-related emissions from drones. Manufacturing, battery production, warehouse construction, refrigeration leakage, and food-waste disposal fall outside the analytical boundary [6]. This narrower scope aligns with tactical routing decisions but precludes interpretation as a full life-cycle assessment; the limitation is explicitly acknowledged.

2.4. Multi-Objective Metaheuristics

Adaptive large-neighborhood search selects among destroy and repair operators using performance feedback. It has been demonstrated that multiple competing neighborhoods can provide robust search behavior for pickup-and-delivery problems with time windows [12]. For emissions-aware routing, ALNS has been combined with specialized route evaluation. These features make ALNS attractive for the present problem because feasibility failures arise from distinct mechanisms: payload overflow, endurance violation, forbidden arcs, missed synchronization, and soft-window cost escalation.

NSGA-II combines nondominated sorting with crowding distance [13]. Hypervolume reflects dominated objective-space coverage, whereas generational distance measures proximity to a reference front. Both require common normalization and transparent reference choices.

The remaining gap lies at the intersection of these streams [14]. Existing work provides mature components for synchronized truck-drone routing, perishability, payload-aware emissions, and Pareto search, but fewer models integrate all four with simultaneous delivery and pickup, demand allocation, dual-network restrictions, and multiple drones. The proposed formulation and operators are designed specifically for this intersection.

3. Problem Definition

3.1. Network and Service Setting

Let $G^g = (V, A^g)$ be the directed ground graph and $G^a = (V, A^a)$ the directed air graph [15]. The node set $V = \{0\} \cup C$ includes depot 0 and customer set C. Ground arc set A^g excludes prohibited truck movements; air arc set A^a excludes infeasible flights following conservative screening of airspace limitations and obstacle-related operational requirements. A set K of refrigerated trucks is stationed at the depot. Each truck k carries a set D_k of compatible drones, and D denotes the union of all such drone sets.

For a feasible ground arc (i,j), d_{ij}^g denotes distance and $\tau_{ij}^g(T)$ denotes time-dependent truck travel time; d_{ij}^a and τ_{ij}^a denote the corresponding air distance and drone flight time [16]. Truck k has payload capacity Q_k. Drone d has payload capacity Q_d and a usable per-sortie energy budget B_d.

Customer i requires delivery quantity q_i^+ and pickup quantity q_i^-. Delivery and pickup demands may be split between a truck and a drone when both quantities and operational policies permit. Each allocated portion is served exactly once, and the sum of allocations equals the total requirement. Each customer has a soft time window $[e_i, l_i]$. Service outside this interval remains feasible but incurs an early or late penalty [17]. The product delivered to customer i has unit value p_i and quality-decay rate λ_i.

The service duration at customer i is denoted by s_i.

A drone sortie begins at a node visited by its carrier truck, serves one eligible customer, and ends at the same or a subsequent truck node. The truck and drone operate concurrently [11]. If one vehicle arrives at the recovery node first, it waits for the other. A sortie is feasible only if payload, energy, air-arc, launch, recovery, and timing conditions are satisfied. All vehicles return to the depot upon completion of assigned tasks.

3.2. Assumptions and Accounting Boundary

The model operates under the following assumptions.

1. Planning is tactical and static within a single dispatch horizon; customer demand volumes and nominal time-dependent travel times are assumed known at route generation, while uncertainty is assessed through ex post congestion scenarios.
2. The depot maintains sufficient inventory, charging infrastructure, and handling capacity for the modeled horizon; drone recharging or battery exchange occurs while onboard the truck between sorties, with associated turnaround time incorporated into launch or recovery service time.
3. Trucks sustain required cold-chain conditions; however, product quality degrades over elapsed time according to a calibrated first-order function, without explicit modeling of temperature excursions.
4. Delivery and pickup operations may be performed during the same visit; truck load is updated on every traversed arc, and for each drone sortie, both outbound delivery mass and return pickup mass must individually satisfy vehicle capacity and energy constraints.
5. Restricted arcs are excluded from the relevant graph; regulatory authorization is not inferred by the model, which assumes all retained air arcs are operationally feasible and legally permissible for the planning scenario.
6. Operational emissions encompass truck fuel combustion and grid-derived electricity used for drone charging; embodied emissions, facility energy consumption, refrigerant leakage, and end-of-life impacts are excluded from scope.
7. The reported case data represent aggregated outputs provided in the source manuscript; underlying commercial order records and executable implementation details were not available for this revision.

4. Multi-Objective Mathematical Formulation

4.1. Objective Vector

The feasible decision set is denoted by Ω. The model seeks a Pareto-efficient solution to the following vector minimization problem:

Here, Z_1, Z_2, and Z_3 represent economic cost, freshness-loss cost, and operational CO_2-equivalent emissions, respectively [18].

$$\min_{x \in \Omega} F(x) = \left(Z_{1(x)}, Z_{2(x)}, Z_{3(x)}\right). \qquad (1)$$

Objectives are evaluated independently during optimization. A solution dominates another if it is at least as good in all three objectives and strictly superior in at least one [19].

4.1.1. Economic Fulfilment Cost

Economic cost comprises fixed activation costs for trucks and drones, truck fuel or distance-related expenses, drone electricity consumption, synchronization waiting time between trucks and drones, and penalties for deviations from prescribed time windows.

The binary variable x_{ijk} equals 1 if truck k traverses ground arc (i,j), and u_{ijhd} equals 1 if drone d launches from i, serves customer j, and is recovered at h.

$$Z_1 = \sum_k f_k y_k + \sum_d f_d y_d + \sum_{(k,i,j)} c_{ij}^{g} x_{ijk} + \sum_{(d,i,j,h)} c_{ijh}^{a} u_{ijhd} + c^w W + \sum_{i} (\pi_i^E a_i + \pi_i^L b_i) . \quad (2)$$

Here, y_k and y_d indicate whether a truck or drone is deployed; c_{ij}^{g} is derived from a payload-sensitive fuel consumption model; c_{ijh}^{a} accounts for electricity usage and handling per drone sortie; W represents total synchronization waiting time; and π_i^E and π_i^L denote early and late penalty coefficients. Nonnegative variables a_i and b_i quantify earliness and lateness, respectively, satisfying the standard deviation constraints [20].

$$a_i \geq e_i - T_i,\ b_i \geq T_i - l_i,\ a_i \geq 0,\ b_i \geq 0. \quad (3)$$

When a customer's demand is served across multiple transport modes, T_i represents the contractually binding completion time. A conservative definition takes the later of the truck and drone completion times. If contractual obligations apply separately to each portion, mode-specific penalties may substitute this maximum without altering the underlying routing structure [21].

Carbon pricing is excluded from Z_1 in the base tri-objective formulation to prevent double-counting emissions—once as a physical environmental objective and again as a monetary cost. For policy sensitivity analysis, the decision cost is evaluated as $Z_{1(p_c)} = Z_1 + p_c Z_3$, where p_c denotes the scenario-specific carbon price, thereby maintaining conceptual separation between emission quantities and their economic valuation [22].

4.1.2. Freshness-Loss Cost

For first-order deterioration, the remaining quality fraction after elapsed time Δt is $\exp(-\lambda_i \Delta t)$. The monetized loss for delivered quantity q is therefore $p_i q[1 - \exp(-\lambda_i \Delta t)]$. With split delivery, the truck and drone portions are evaluated at their respective service times:

The variables T_{ik}^{T} and T_{id}^{D} denote the truck and drone service times for customer i, respectively [23].

$$Z_2 = \sum_i p_i \left\{ \sum_k q_{ik}^{T+} \left[1 - \exp\left(-\lambda_{i(T_{ik}^{T} - t_0)}\right)\right] + \sum_d q_{id}^{D+} \left[1 - \exp\left(-\lambda_{i(T_{id}^{D} - t_0)}\right)\right] \right\}. \quad (4)$$

The formulation applies to delivered fresh products [6, 14]. Pickups—such as returns, packaging, or reverse-logistics items—are included in capacity propagation but are not automatically assigned fresh-product value. If pickups also deteriorate, an analogous term may be introduced using their specific value and exposure time.

The decay rate λ_i should be estimated from product-specific shelf-life or temperature-history data; using a single uniform value represents a simplification [16].

4.1.3. Operational Carbon Emissions

Truck fuel consumption per unit distance is approximated by linear interpolation between empty and fully loaded consumption rates θ_k^0 and θ_k^F. For arc (i,j), the load ratio is $\frac{L_{ijk}}{Q_k}$. Truck emissions are calculated accordingly [15, 20].

$$E^T = EF_f \sum_{(k,i,j)} d_{ij}^{g} x_{ijk} \left[\theta_k^0 + (\theta_k^F - \theta_k^0)\left(\frac{L_{ijk}}{Q_k}\right)\right] . \quad (5)$$

EF_f converts fuel use to kilograms of CO_2-equivalent [9]. Drone electricity demand depends on the energy required for both outbound and return legs, including payload effects.

$$E^D = EF_e \sum_{d,i,j,h} \left[E_d^{a(i,j,q_{jd}^{D+})} + E_d^{a(j,h,q_{jd}^{D-})}\right] u_{ijhd} . \quad (6)$$

EF_e represents the electricity emission factor [6, 18]. The third objective is formulated as follows.

$$Z_3 = E^T + E^D. \quad (7)$$

Equations (5)–(7) define an operational boundary. The truck approximation omits acceleration, road grade, refrigeration load, and ambient temperature effects; the drone term requires aircraft-specific calibration. Fuel-to-emissions conversion may rely on standardized emission factors, while drone emissions depend on local grid electricity intensity [19].

4.2. Assignment and Route Continuity

Demand conservation allows partial service but requires full assignment of all demand quantities [3].

Let q_{ik}^{T+} and q_{ik}^{T-} denote the delivery and pickup quantities assigned to truck k at customer i, and q_{id}^{D+} and q_{id}^{D-} the corresponding quantities assigned to drone d.

$\sum_k q_{ik}^{T+} + \sum_d q_{id}^{D+} = q_i^+,\ \sum_k q_{ik}^{T-} + \sum_d q_{id}^{D-} = q_i^-,\ \forall i \in C.$(8)

Allocation is tied to a physical visit: if truck k is assigned zero quantity at i, no visit is required; otherwise, one inbound and one outbound ground arc must be included. Standard depot connectivity and flow-balance conditions apply.

$\sum_j x_{0jk} = y_k,\ \sum_i x_{i0k} = y_k,\ \forall k \in K,$ (9)

$\sum_i x_{ihk} = \sum_j x_{hjk},\ \forall h \in C, k \in K.$ (10)

4.3. Dynamic Payload and Capacity

Let L_{ijk} denote the payload after service at node i and before service at node j. For a used truck arc, the load evolves as delivered quantity is unloaded from the vehicle and pickup quantity is loaded onto it:

$L_{jhk} \geq L_{ijk} - q_{jk}^{T+} + q_{jk}^{T-} - M(1 - x_{jhk}),\ \forall\, feasible\ consecutive\ arcs.$ (11)

$0 \leq L_{ijk} \leq Q_k x_{ijk}.$ (12)

The truck departs carrying the full assigned delivery mass and returns bearing the collected pickup mass:

$L_{0jk} = \sum_i q_{ik}^{T+},\ L_{i0k} = \sum_i q_{ik}^{T-},\ for\ each\ used\ truck\ route.$ (13)

Equivalent upper and lower propagation inequalities are incorporated into an exact linear formulation. The route evaluator computes loads deterministically and discards any route where the intermediate load violates capacity constraints [2]. Drone outbound and inbound payloads satisfy

$q_{jd}^{D+} \leq Q_d u_{ijhd},\ q_{jd}^{D-} \leq Q_d u_{ijhd}.$ (14)

Using distinct bounds aligns with simultaneous service: the drone completes its outbound delivery before transporting the pickup item on the return leg.

4.4. Time Propagation, Synchronization, and Endurance

Truck service times are propagated along traversed ground arcs.

$T_{jk}^T \geq T_{ik}^T + s_i + \tau_{ij}^g(T_{ik}^T) - M(1 - x_{ijk}).$ (15)

For a sortie (i,j,h,d), the drone's service and recovery times must satisfy timing consistency constraints.

$T_{jd}^D \geq T_{ik}^T + t_d^{launch} + \tau_{ij}^a - M(1 - u_{ijhd}),$ (16)

$R_{hd} \geq T_{jd}^D + s_j + \tau_{jh}^a + t_d^{recover} - M(1 - u_{ijhd}).$ (17)

The carrier truck may depart recovery node h only after both the truck and the drone are available [17].

$T_{hk}^{depart} \geq \max(T_{hk}^{arrive}, R_{hd})\, for\ every\ active\ sortie\ recovered\ at\ h.$ (18)

In a mixed-integer formulation, the maximum operator is replaced by linear lower bounds. Waiting time arises from the absolute temporal mismatch between the two arrival processes and contributes to W in Equation (2). A drone cannot be scheduled for overlapping sorties, and the number of concurrent launches or recoveries must not exceed the physical resources carried by the truck.

Sortie energy consumption must remain within the drone's usable battery capacity [2].

$E_d^{a(i,j,q_{jd}^{D+})} + E_d^{a(j,h,q_{jd}^{D-})} + E_d^{reserve} \leq B_d + M(1 - u_{ijhd}).$(19)

In Equation (19), B_d denotes the usable sortie-energy budget of drone d, $E_d^{reserve}$ represents the contingency reserve, and M is a sufficiently large constant.

The reserve term accounts for wind effects, battery aging, maneuvering demands, and operational contingencies. Ground and air restrictions are enforced by defining x_{ijk} only for (i,j) in A^g, and u_{ijhd} only when both corresponding air legs belong to A^a. This graph-based constraint formulation is more robust and concise than prohibiting variables via forced zero assignments (As shown in Figure 1).

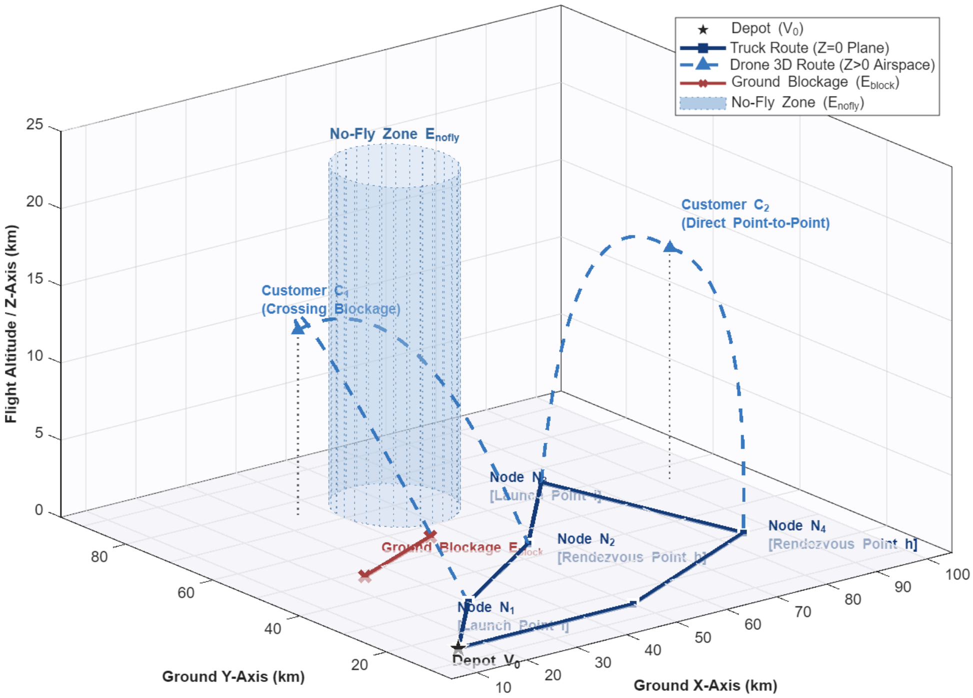

Figure 1. Schematic Truck-Multi-Drone Routing with a Ground Blockage and a No-Fly Region (Not to Scale).

5. Multi-Objective Adaptive Large-Neighborhood Search

5.1. Solution Representation and Initialization

A solution comprises ordered depot-to-depot truck routes, customer-level mode allocations, and drone sorties characterized by carrier truck, drone identifier, launch node, served customer, and recovery node. The decoder updates truck load, arrival time, service time, drone availability, battery consumption, and synchronization waiting in real time. This integrated representation ensures route evaluation reflects current payload and timing conditions following any neighborhood modification.

Initialization occurs in two phases [8]. First, a time-oriented greedy insertion constructs feasible truck routes using marginal travel cost, time-window slack, and dynamic capacity constraints. Second, a drone-allocation phase identifies eligible customers and substitutes selected truck visits—or portions thereof—with feasible drone sorties when such substitution improves at least one normalized objective without causing unacceptable degradation in others. Multiple randomized initialization trials mitigate sensitivity to the initial greedy construction. All generated feasible solutions are evaluated for inclusion in the external nondominated archive.

5.2. Destroy Operators

The destroy stage eliminates customers, demand portions, sorties, or route fragments using six distinct operators [23].

1. Random removal provides diversification without embedding a directional bias.
2. Marginal-cost removal targets customers whose removal most reduces economic cost, including waiting and time-window penalties.
3. High-freshness-loss removal prioritizes delivered portions with large $p_i q_{i[1-\exp(-\lambda_i \Delta t)]}$, creating opportunities to serve them earlier or by drone.

4. Payload-carbon removal targets customers or route segments with a high contribution to the payload-distance term in Equation (5). Large early deliveries are candidates for resequencing, while pickups that create sustained heavy loads may be postponed when service constraints allow.
5. Boundary-risk removal selects customers near blocked ground arcs, restricted air polygons, or low-slack drone sorties. Removing a connected set around the boundary helps the repair stage switch mode or select another launch-recovery pair.
6. Split-skeleton removal breaks a coupled truck-drone allocation involving one or more split customers, including its launch and recovery anchors. This operator is necessary because changing only the served customer may leave an infeasible or unnecessarily long synchronization structure.

Related removal based on distance, time-window overlap, product decay rate, and common restriction exposure is also applied as a controlled variant. Removal size is randomized within a range that grows temporarily after archive stagnation.

5.3. Repair operators

The repair stage reconstructs a complete feasible plan using five operators.

1. Greedy insertion selects the feasible location with the smallest normalized marginal deterioration across the three objectives.
2. Regret-k insertion prioritizes a customer when delaying its insertion would sharply worsen the second- or third-best option. This is useful for tight time windows and scarce feasible drone sorties.
3. Split-demand recomposition jointly chooses truck and drone quantities. Candidate splits are screened by truck and drone capacity, product eligibility, handling policy, and the arrival-time difference between portions.
4. Safe-air insertion enumerates feasible launch-customer-recovery triples on the carrier route, removes any triple intersecting a no-fly arc, and ranks the remainder by energy, freshness, and synchronization cost.
5. Synchronization repair searches downstream recovery nodes and limited truck-route shifts to minimize total waiting while respecting endurance and drone availability. When no feasible recovery exists, the customer is returned to truck service or the sortie is moved to another compatible drone.

All insertions are evaluated incrementally but confirmed by a full decoder before acceptance. A solution with an impossible route, capacity excess, overlapping drone sorties, missing quantity, prohibited arc, or insufficient reserve energy is rejected. Soft time-window violations are permitted and costed.

5.4. Archive, acceptance, and adaptive weights

The external archive A stores mutually nondominated solutions. After a feasible candidate s' is decoded, dominated archive members are removed and s' is inserted if it is not dominated. When the archive exceeds its capacity, solutions in crowded objective-space regions are removed while extreme solutions are protected. Objective values are normalized using rolling ideal and nadir estimates so that cost measured in dollars does not overwhelm emissions measured in kilograms.

The current search state is allowed to move beyond strict dominance. At each iteration, a random weight vector defines a normalized achievement scalarizing function. A candidate that improves this function is accepted; a deteriorating candidate may be accepted with a simulated-annealing probability that decreases with temperature. Nondominated candidates are always offered to the archive. This combination maintains exploration while the archive preserves Pareto progress.

Destroy and repair operators are selected by roulette wheel. Let ω_r be the weight of operator r, π_r its accumulated score in a segment, and n_r its number of uses. At the end of a segment, the update is

$$\omega_r \leftarrow (1-\rho)\omega_r + \rho\left(\frac{\pi_r}{\max(1,n_r)}\right), \qquad (20)$$

where ρ is the reaction factor. Higher rewards are assigned when an operator creates a new archive member, smaller rewards when it improves the current scalarizing function, and no reward when it repeatedly generates infeasible or rejected solutions. A positive minimum weight prevents permanent loss of exploration.

5.5. Termination and output

The reported configuration uses 500 MO-ALNS iterations, an archive capacity of 100, and 10 independent runs. The original draft also listed a population of 100, crossover probability 0.8, and mutation probability 0.2; those are NSGA-II parameters and are reported only for the benchmark, because MO-ALNS does not use genetic crossover or mutation. Termination occurs at the iteration limit or after a specified archive-stagnation threshold. The output is the pooled nondominated archive after duplicate removal and objective normalization.

6. Computational Study

6.1. Scenario Construction and Data Provenance

The numerical study uses a Manhattan-calibrated urban scenario with a single depot, customer clusters, simultaneous delivery and pickup, soft time windows, congested ground travel, blocked road arcs, and screened air restrictions. Road distances and travel-time estimates were described in the source manuscript as map-derived and traffic-adjusted. Airspace screening was described as consistent with publicly available aviation regulatory information and open-map features. Cost parameters were calibrated using publicly available energy and operational cost categories, including fuel and electricity price series and wage data from national statistical sources. Carbon conversion factors were aligned with the corresponding year's official environmental reporting guidelines. Recent studies conducted in China on weight-sensitive pickup and delivery operations, reverse-logistics scheduling, and heterogeneous cold-chain vehicle fleets provide additional regional context for the selected operational conditions.

The source draft characterized the order set as one week of anonymized commercial orders. However, the customer-level records, aggregation procedure, coordinates, exact access date for dynamic pricing data, and usage permissions were not supplied with the document. The revised paper therefore uses the more precise term "Manhattan-calibrated scenario" rather than presenting the study as independently verifiable real-company evidence. The aggregated outcomes remain useful for internal comparison because all tested modes and algorithms are evaluated under the same stated scenario.

Benchmark logic follows the spatial and time-window conventions of widely adopted benchmark instances, but Tables report the Manhattan-calibrated case. For a reproducible submission, the authors should release at minimum the de-identified node table, q_i^+ and q_i^- values, time windows, decay parameters, ground and air travel matrices, restricted-arc lists, vehicle specifications, random seeds, source code, compiler or interpreter version, processor details, and run-level outcomes.

6.2. Experimental Protocol and Metrics

MO-ALNS is executed independently 10 times for 500 iterations, with the external archive limited to 100 solutions [13]. NSGA-II employs a population size of 100, crossover probability of 0.8, mutation probability of 0.2, and the same nominal iteration budget. Both algorithms optimize the same three objectives and adhere to identical operational requirements. Benchmarking relies on hypervolume and generational distance metrics. Since the true Pareto front is unavailable, the reference front is constructed from the union of all nondominated solutions across all algorithm runs. Prior to indicator calculation, each objective is normalized, and a single common dominated reference point is applied for hypervolume computation.

The source tables report mean values for performance indicators and runtime but omit standard deviation, confidence intervals, random seeds, and paired run-level data. Consequently, the analysis presents percentage differences without asserting statistical significance. Runtime is reported solely as a descriptive metric, given the absence of details regarding processor specifications and implementation [21].

The truck-only (TO) baseline excludes drone usage while preserving customer demand volumes, ground-based operational rules, vehicle cost parameters, soft time windows, and payload-dependent truck emissions. The truck-drone collaborative (TDC) configuration implements the full integrated model. This controlled comparison isolates the contribution of aerial support within the defined scenario, though it does not incorporate alternative delivery modes such as electric vans, cargo bikes, micro-hubs, or adjusted time window policies.

6.3. Truck-Only Versus Collaborative Delivery

Table 1 compares the best reported fulfilment outcomes after 500 iterations. Truck-drone collaboration reduces cost by USD 266.58, freshness-loss cost by USD 131.32, and operational emissions by 8.45 kg CO_2e. The time-window violation rate declines from 34.5% to 8.2%, representing a reduction of 26.3 percentage points or 76.2% relative to the truck-only baseline. Fourteen drone sorties are deployed.

Table 1. Truck-only and Truck-Drone Collaborative Fulfilment Performance.

Performance measure	Symbol	Truck-only	Collaborative	Change
Total fulfilment cost (USD)	Z_1	1,425.60	1,159.02	-18.70%
Freshness-loss cost (USD)	Z_2	310.45	179.13	-42.30%
Operational emissions (kg CO2e)	Z_3	48.25	39.80	-17.51%
Orders outside soft windows	$R_{timeout}$	34.50%	8.20%	-26.3 percentage points
Drone sorties	N_d	0	14	+14

The largest proportional improvement occurs in freshness preservation. This aligns with the operational principle: drone sorties deliver maximum value when assigned to small, time-sensitive deliveries that would otherwise necessitate inefficient truck detours through congested areas. Cost reduction arises because savings from avoided truck travel and lateness penalties outweigh drone activation, electricity consumption, and coordination overhead. Emissions decrease due to shorter truck routes and reduced payload on certain arcs, while drone electricity use remains comparatively negligible within the defined operational boundary [5].

6.4. Pareto Trade-Offs

Table 2 presents three nondominated solutions. Solution A minimizes economic cost, Solution B prioritizes freshness preservation, and Solution C minimizes operational carbon emissions [22]. The comparative values illustrate the limitations of aggregating these objectives into a single weighted score.

Table 2. Representative Nondominated Solutions on the Pareto Front.

Representative solution	Cost Z_1 (USD)	Freshness loss Z_2 (USD)	Emissions Z_3 (kg CO2e)	Truck distance (km)	Drone distance (km)
A: cost-oriented	1,085.50	217.45	42.10	85.4	12.5
B: freshness-oriented	1,424.15	145.20	38.65	72.8	65.2
C: carbon-oriented	1,210.30	185.60	35.53	68.5	48.4

Solution A employs relatively limited drone distance. It is 10.3% less costly than Solution C and 23.8% less costly than Solution B, yet its freshness loss is 17.2% greater than that of Solution C and 49.8% greater than that of Solution B. The route accepts extended product exposure for certain deliveries because additional drone sorties and schedule synchronization would incur higher economic costs than the corresponding freshness improvements under the economic objective [18].

Solution B reduces freshness-loss cost by USD 72.25 compared to Solution A. It requires more than five times the drone distance of Solution A and incurs the highest economic cost [11]. The increased air service accelerates priority orders, but necessitates greater truck involvement in drone launch and recovery operations. The model explicitly accounts for associated waiting and handling delays rather than treating drone travel as decoupled from the truck schedule.

Solution C achieves the lowest operational emissions, with a result of 35.53 kg CO2e—15.6% below Solution A and 8.1% below Solution B. Although Solution B uses substantially more drone distance, it does not yield the lowest carbon outcome, confirming that flight speed and volume alone are insufficient proxies for emissions. Solution C reduces total truck distance and adopts a service sequence that unloads high-volume deliveries earlier, thereby lowering the payload-distance integral in Equation (5). This "fast-unloading" behavior arises from route-sequencing effects: a marginally longer or less freshness-optimized local movement can reduce emissions across multiple downstream arcs.

6.5. Algorithm Comparison

Table 3 reports aggregate MO-ALNS and NSGA-II performance. MO-ALNS increases hypervolume (HV) from 0.684 to 0.781, a 14.18% improvement, and reduces generational distance (GD) from 0.045 to 0.034, a 24.44% improvement [16]. These changes indicate broader dominated solution coverage and closer proximity to the pooled reference front. MO-ALNS reaches its reported convergence region near iteration 180, whereas NSGA-II converges near iteration 310.

Table 3. Reported Mo-alns and Nsga-ii Performance Comparison.

Algorithm	Hypervolume	Generational distance	Mean runtime (s)	Approximate convergence iteration
NSGA-II	0.684	0.045	115.4	about 310
MO-ALNS	0.781	0.034	128.6	about 180

Relative difference	+14.20%	-24.40%	+11.44%	earlier by about 130 iterations

The improvement aligns with operator specialization: boundary-risk removal, safe-air insertion, and synchronization repair directly modify coupled launch-recovery structures, while the archive maintains diverse trade-off solutions.

Runtime comparison reveals a nuanced trade-off previously underemphasized. MO-ALNS is not faster in wall-clock time; it requires approximately 13.2 s more per run—about 11.4% slower. Its advantages lie in superior objective-space quality and earlier iteration-level convergence. Without matched hardware specifications, implementation details, or uncertainty quantification, the data support only scenario-specific performance claims, not universal algorithm ranking.

6.6. Carbon-Price Sensitivity

Carbon-price sensitivity is evaluated by incorporating $p_c Z_3$ into the decision cost and re-optimizing under four relative price scenarios: 50% below the reference level, the reference level, 50% above, and 100% above. Using relative price levels avoids assumptions of universal applicability or temporal stability of a single market price. Table 4 presents the selected cost-oriented solution for each scenario.

Table 4. Carbon-price Sensitivity of Fleet Allocation and Fast Unloading.

Carbon-price scenario	Decision cost (USD)	Emissions (kg CO2e)	Truck task share	Drone task share	Fast-unloading trigger rate
Low (-50%)	1,120.45	45.30	88%	12%	15%
Reference	1,159.02	39.80	78%	22%	42%
High (+50%)	1,234.60	33.15	65%	35%	76%
Very high (+100%)	1,352.18	29.40	54%	46%	91%

From the low to the very high carbon-price scenario, the reported decision cost increases by 20.7%, while total emissions decrease by 35.1%. The drone task share rises by 34 percentage points, and the fast-unloading trigger rate increases by 76 percentage points. These trends reflect two adaptive responses to higher carbon valuation: first, a modal shift—more eligible tasks are assigned to electric drones; second, a sequential adjustment—the truck prioritizes high-delivery customers earlier in the route to reduce downstream payload.

Given that only four scenario points are examined, the results indicate a monotonic association rather than establishing nonlinear causal relationships. Factors such as a high-carbon electricity grid, larger drone specifications, or adverse weather conditions could attenuate the observed modal shift.

6.7. Congestion Robustness

The robustness test adjusts truck travel speed using multiplicative congestion factors. The source draft referenced a combination of normal and uniform variations but specified only maximum factor values. The revised interpretation treats these as scenario bounds rather than a fully defined probabilistic distribution. Table 5 compares TO and TDC.

Table 5. Congestion-resilience Comparison under Travel-Time Disturbance.

Congestion severity	TO timeout rate	TDC timeout rate	TDC cost deterioration	TDC runtime (s)
Mild (ξ_{max} 2)	18.50%	4.20%	2.10%	135.2
Moderate (ξ_{max} 5)	42.10%	9.80%	5.60%	142.8
Severe (ξ_{max} 8)	76.40%	15.30%	11.40%	156.4

Under severe congestion conditions, TDC maintains a timeout rate of 15.3%, compared with 76.4% for TO. The absolute difference is 61.1 percentage points [18]. TDC decision cost increases by 11.4%, and runtime remains below 160 s in the reported runs. Drone routes serve as an aerial buffer since their travel times are unaffected by ground congestion, while the adaptive search dynamically reassigns customers whose truck service becomes suboptimal.

This test modifies ground travel speed only; the result therefore demonstrates resilience to traffic congestion, not general robustness against weather, battery limitations, communication failures, or airspace constraints [9] (As shown in Figure 2).

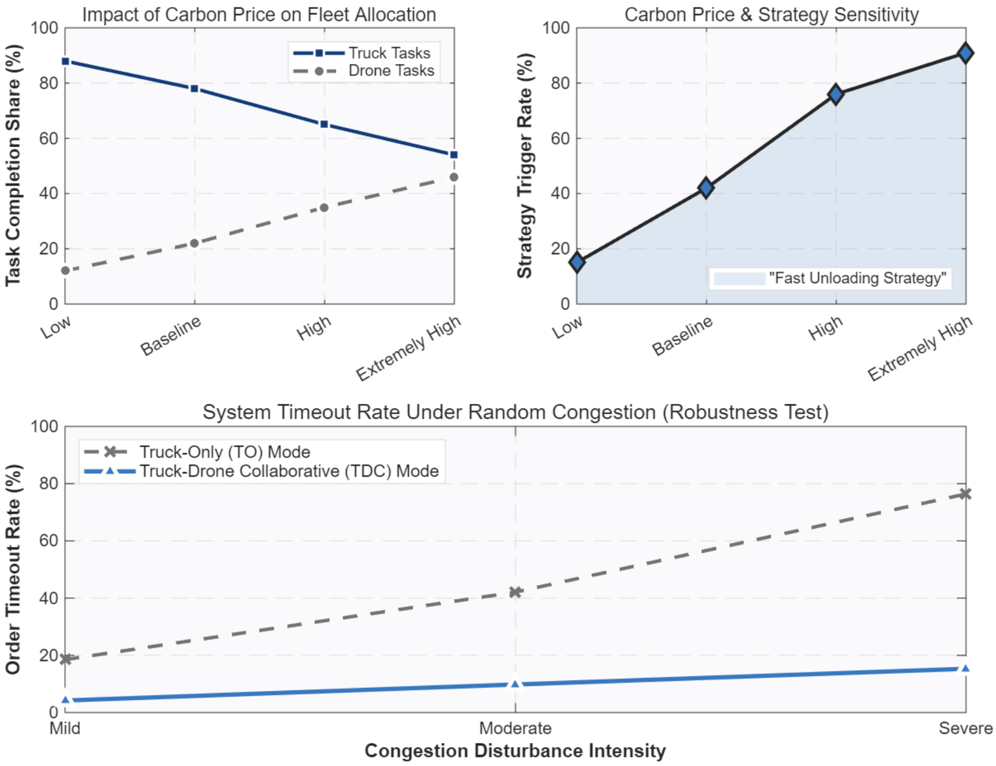

Figure 2. Reported Carbon-Price Sensitivity and Congestion-Resilience Patterns.

7. Discussion

7.1. Theoretical Implications

The results indicate that payload functions as a dynamic routing state rather than a static operational limit [11]. In simultaneous delivery and pickup operations, the customer sequence governs both solution feasibility and the cumulative emissions along subsequent arcs. The rapid-unloading behavior observed under carbon-conscious scenarios arises directly from this interdependence. A distance-minimizing model fails to capture this mechanism, as it does not account for the timing of mass removal. This insight extends pollution-routing principles to synchronized truck-drone cold-chain logistics.

The study further clarifies the functional role of drones in perishable goods distribution. Their primary advantage lies not in universal acceleration but in targeted decoupling from ground-based routing. A drone sortie becomes advantageous when it avoids a costly truck detour, safeguards high-priority or rapidly deteriorating items, or maintains tight time-window compliance without inducing excessive truck idle time. This accounts for the higher drone flight distance in freshness-optimized solutions compared to the more balanced air allocation in carbon-optimized solutions. Freshness preservation, emission reduction, and drone utilization are interrelated yet distinct performance dimensions.

From an algorithmic perspective, the comparative analysis underscores the importance of aligning neighborhood structures with the nature of constraint interdependencies. In standard vehicle routing problems, removing a customer is a localized operation. In integrated truck-drone routing, the same action may disrupt multiple coordinated elements—including drone launch and recovery points, drone scheduling, truck waiting periods, dual payload trajectories, and several time windows. Operators designed to remove and reconstruct this interdependency framework enable more effective exploration of feasible solution spaces than those overlooking such couplings. This advantage is evident in hypervolume (HV) and generational distance (GD) metrics, though broader validation remains warranted.

7.2. Managerial Implications

First, firms should implement a customer-eligibility layer to constrain drone assignment, rather than permitting the optimizer to allocate every small order to a drone. Eligibility criteria must encompass package mass and dimensions, product sensitivity, safe handoff capability, customer acceptance, airspace availability, weather conditions, property access, and recovery feasibility. The optimization process then selects from among operationally viable options.

Second, dispatch systems must dynamically update payload status after each delivery and pickup. A payload-aware routing strategy may prioritize a larger delivery over a geographically nearer small-order customer. This sequencing principle gains greater operational significance under rising fuel or carbon costs, though it must be carefully balanced against product freshness requirements and service-level commitments [6].

Third, managers should select solutions from the Pareto-optimal set using clearly defined, policy-driven constraints. Examples include a maximum allowable freshness degradation, an absolute carbon emission limit, a minimum required on-time delivery rate, or an upper threshold on daily drone sorties. Such explicit constraints enhance auditability compared to opaque weighted objectives and enable the same optimization framework to accommodate diverse business priorities.

7.3. Limitations and Validity Threats

The most important limitation is reproducibility. The aggregated tables cannot be independently regenerated without access to the customer matrix, route graphs, parameter file, source code, hardware configuration, and random seeds. Consequently, the manuscript does not assert statistical significance or external validation. A publishable empirical package should report run-level hypervolume (HV), generational distance (GD), runtime, and objective values, followed by paired nonparametric tests and effect sizes across heterogeneous instance classes [5].

Second, the operational emission boundary is narrower than a full life-cycle boundary. Emissions associated with drone battery production and replacement, additional charging infrastructure, warehousing requirements, refrigeration energy consumption, and food-waste outcomes are excluded. Since freshness improvement may reduce spoilage, a broader system analysis could strengthen or alter the carbon impact conclusion. Similarly, using an average grid emission factor overlooks time-varying marginal electricity emissions.

Third, the uncertainty test perturbs ground travel only. A field-ready model should account for correlated traffic congestion, stochastic order arrivals, weather-dependent flight duration and energy consumption, temporary air traffic restrictions, service-time variability, and battery degradation. Methodologies such as two-stage stochastic programming, robust optimization, or rolling-horizon rescheduling could integrate these factors.

Fourth, the model treats the no-fly graph as static and fully known. In practice, regulatory restrictions distinguish between flight prohibition zones and take-off/landing limitations, and authorization may vary by time and location. The route planner must therefore interface dynamically with real-time operational approvals [8]. The schematic air corridor in Figure 1 is illustrative and does not represent an authorized Manhattan route.

Finally, the comparison set is limited [2, 12]. Alternative delivery modes—including cargo bicycles, electric vans, parcel lockers, curbside micro-hubs, relaxed time windows, and demand consolidation—may yield lower cost or lower carbon outcomes. Future studies should evaluate these options under consistent service-level and life-cycle boundary assumptions.

8. Conclusions

This paper develops a tri-objective framework for truck-multi-drone urban cold-chain routing with simultaneous delivery and pickup, demand allocation across vehicles, soft time windows, ground and air restrictions, synchronization, perishable-product decay, and payload-dependent operational emissions. The MO-ALNS combines a nondominated archive with adaptive, problem-specific neighborhoods that target freshness loss, payload-carbon contribution, restricted-network boundaries, service distribution across vehicles, safe air insertion, and launch-recovery synchronization.

In the Manhattan-calibrated scenario, collaborative routing reduces reported economic cost by 18.70%, freshness-loss cost by 42.30%, operational emissions by 17.51%, and time-window violations by 26.3 percentage points relative to truck-only delivery. The Pareto analysis shows that the least-cost, freshest, and lowest-carbon schedules require materially different allocations and sequences. Carbon-price sensitivity suggests both a shift toward drone service and more frequent early unloading of large deliveries. The congestion test indicates that aerial support can preserve service when the ground network degrades. MO-ALNS improves HV and GD relative to NSGA-II, but it also requires more wall-clock time in the reported averages.

The conclusions are conditional on the supplied scenario and operational accounting boundary. Before journal submission or deployment, the model should be supported by a de-identified reproducibility package, run-level statistical analysis, aircraft-specific energy calibration, and current regulatory screening. Future work should address rolling-horizon orders, correlated ground and air uncertainty, multiple depots, heterogeneous fleets, temperature-dependent decay, refrigeration energy, and life-cycle carbon. These extensions would move the framework from a promising scenario model toward a verifiable decision-support system for resilient low-carbon cold chains.

Data and Code Availability: The numerical tables in this manuscript are based on aggregate case-study outputs supplied in the source document. Customer-level commercial orders, complete network matrices, executable source code, random seeds, and run-level observations were not included in the materials available for this revision and therefore cannot be distributed with this version. The mathematical formulation and the reporting requirements in Sections 3–6 define the minimum information needed for a reproducible release.

Conflict of Interest: The authors declare no conflict of interest. This statement should be confirmed by all authors before submission.

References

1. P. Bouman, N. Agatz, and M. Schmidt, "Dynamic programming approaches for the traveling salesman problem with drone," *Networks*, vol. 72, no. 4, pp. 528–542, 2018.
2. D. Schermer, M. Moeini, and O. Wendt, "A branch-and-cut approach and alternative formulations for the traveling salesman problem with drone," *Networks*, vol. 76, no. 2, pp. 164–186, 2020.
3. Q. M. Ha, Y. Deville, Q. D. Pham, and M. H. Hà, "On the min-cost traveling salesman problem with drone," *Transportation Research Part C: Emerging Technologies*, vol. 86, pp. 597–621, 2018.
4. A. Kumar, V. Prybutok, and V. K. R. Sangana, "Environmental implications of drone-based delivery systems: A structured literature review," *Clean Technologies*, vol. 7, no. 1, p. 24, 2025.
5. W. C. Chiang, Y. Li, J. Shang, and T. L. Urban, "Impact of drone delivery on sustainability and cost: Realizing the UAV potential through vehicle routing optimization," *Applied Energy*, vol. 242, pp. 1164–1175, 2019.
6. E. Demir, T. Bektaş, and G. Laporte, "An adaptive large neighborhood search heuristic for the pollution-routing problem," *European Journal of Operational Research*, vol. 223, no. 2, pp. 346–359, 2012.
7. C. I. Hsu, S. F. Hung, and H. C. Li, "Vehicle routing problem with time-windows for perishable food delivery," *Journal of Food Engineering*, vol. 80, no. 2, pp. 465–475, 2007.
8. E. Demir, T. Bektaş, and G. Laporte, "A review of recent research on green road freight transportation," *European Journal of Operational Research*, vol. 237, no. 3, pp. 775–793, 2014.
9. A. Osvald and L. Z. Stirn, "A vehicle routing algorithm for the distribution of fresh vegetables and similar perishable food," *Journal of Food Engineering*, vol. 85, no. 2, pp. 285–295, 2008.
10. P. Amorim and B. Almada-Lobo, "The impact of food perishability issues in the vehicle routing problem," *Computers & Industrial Engineering*, vol. 67, pp. 223–233, 2014.
11. S. H. Chung, B. Sah, and J. Lee, "Optimization for drone and drone-truck combined operations: A review of the state of the art and future directions," *Computers & Operations Research*, vol. 123, p. 105004, 2020.
12. M. M. Solomon, E. K. Baker, and J. R. Schaffer, "Vehicle routing and scheduling problems with time window constraints: Efficient implementations of solution improvement procedures," in *Vehicle Routing: Methods and Studies*, vol. 16, 1988.
13. G. Attenni, V. Arrigoni, N. Bartolini, and G. Maselli, "Drone-based delivery systems: A survey on route planning," *IEEE Access*, vol. 11, pp. 123476–123504, 2023.
14. Y. Li, W. Yang, and B. Huang, "Impact of UAV delivery on sustainability and costs under traffic restrictions," *Mathematical Problems in Engineering*, vol. 2020, no. 1, p. 9437605, 2020.
15. F. A. T. Montané and R. D. Galvão, "Vehicle routing problems with simultaneous pick-up and delivery service," *Opsearch*, vol. 39, no. 1, pp. 19–33, 2002.
16. A. Baldisseri, C. Siragusa, A. Seghezzi, R. Mangiaracina, and A. Tumino, "Truck-based drone delivery system: An economic and environmental assessment," *Transportation Research Part D: Transport and Environment*, vol. 107, p. 103296, 2022.
17. K. Deb, A. Pratap, S. Agarwal, and T. A. M. T. Meyarivan, "A fast and elitist multiobjective genetic algorithm: NSGA-II," *IEEE Transactions on Evolutionary Computation*, vol. 6, no. 2, pp. 182–197, 2002.
18. E. Zitzler, L. Thiele, M. Laumanns, C. M. Fonseca, and F. V. G. Da, "Performance assessment of multiobjective optimizers: An analysis and review," *IEEE Transactions on Evolutionary Computation*, vol. 7, no. 2, pp. 117–132, 2003.
19. Y. Li, H. Chen, and C. Prins, "Adaptive large neighborhood search for the pickup and delivery problem with time windows, profits, and reserved requests," *European Journal of Operational Research*, vol. 252, no. 1, pp. 27–38, 2016.
20. Y. Li, M. K. Lim, W. Xiong, X. Huang, Y. Shi, and S. Wang, "An electric vehicle routing model with charging stations consideration for sustainable logistics," *Industrial Management & Data Systems*, vol. 124, no. 3, pp. 1076–1106, 2024.
21. S. Zhang, C. Guan, Y. Qiu, and N. Wu, "Multi-objective route optimization of urban cold chain distribution using electric and diesel powered vehicles," *Research in Transportation Business & Management*, vol. 49, p. 100969, 2023.
22. F. Y. Vincent, P. H. Hsu, and S. W. Lin, "The cold chain vehicle routing problem in omni-channel retailing," *Expert Systems with Applications*, p. 132564, 2026.
23. L. Zhang, Y. Gao, Y. Sun, T. Fei, and Y. Wang, "Application on cold chain logistics routing optimization based on improved genetic algorithm," *Automatic Control and Computer Sciences*, vol. 53, no. 2, pp. 169–180, 2019.